Entanglement wedge cross section growth during thermalization

Komeil Babaei Velni,[1,3,*] M. Reza Mohammadi Mozaffar,[1,3,†] and M. H. Vahidinia[2,3,‡]

[1]*Department of Physics, University of Guilan, P.O. Box 41335-1914, Rasht, Iran*
[2]*Department of Physics, Institute for Advanced Studies in Basic Sciences (IASBS), P.O. Box 45137-66731, Zanjan, Iran*
[3]*School of Physics, Institute for Research in Fundamental Sciences (IPM), P.O.Box 19395-5531, Tehran, Iran*

(Received 14 March 2023; accepted 9 May 2023; published 25 May 2023)

Motivated by exploring the thermalization process in relativistic and nonrelativistic holographic field theories after a nonlocal quench, we investigate some features in the time evolution of the entanglement wedge cross section (EWCS). This quantity is a possible holographic dual to some nonlocal information measures such as entanglement of purification. In particular, we focus on the time dependence of the EWCS during black hole formation in $(D+2)$-dimensional anti–de Sitter spacetime as well as geometries with Lifshitz and hyperscaling-violating exponents. A combination of analytic and numerical results for large symmetric strip shaped boundary subregions shows that the scaling of the EWCS at early times only depends on the Lifshitz exponent. In addition, this early-growth regime is followed by a linear-growth regime whose velocity depends on the dimensions of spacetime, the Lifshitz exponent, and the hyperscaling parameter. This velocity is the same as the entanglement velocity and for nontrivial dynamical exponent depends on the temperature of the final equilibrium state.

DOI: 10.1103/PhysRevD.107.106014

I. INTRODUCTION

The gauge/gravity duality allows us to quantitatively study surprising new connections between quantum information theory and quantum gravity in recent years, e.g., see reviews [1–3]. In particular, it is now evident that certain geometric quantities in the bulk geometry can be related to the information-theoretic measures of the boundary field theory. In this context, the entanglement entropy (EE) associated with a spatial boundary subregion A is determined by the Ryu-Takayanagi (RT) formula [4]

$$S_A = \min \frac{\mathrm{Area}(\Gamma_A)}{4G_N}, \tag{1.1}$$

where Γ_A is a bulk minimal hypersurface homologous to A, i.e., $\partial\Gamma_A = \partial A$. Moreover, the Hubeny-Rangamani-Takayanagi (HRT) proposal [5] extends this prescription to time-dependent situations by considering extremal hypersurfaces with the same boundary condition. These proposals have stimulated a wide variety of research efforts investigating the properties of entanglement and information measures holographically. An interesting suggestion in this research program is that the entanglement of mixed states in the boundary theory is encoded in a certain codimension-two bulk hypersurface which is called the entanglement wedge cross section (EWCS). Considering a spatial region A in the boundary theory, the entanglement wedge is the bulk region corresponding to the reduced density matrix ρ_A and whose boundary is $A \cup \Gamma_A$. In particular, when the boundary region is the union of two disjoint subregions A_1 and A_2 the boundary of the entanglement wedge is $A_1 \cup A_2 \cup \Gamma_{A_1 \cup A_2}$. For small separations where the connected configuration is favored, the EWCS is defined to be the minimal cross sectional area of the entanglement wedge and is given as follows [6,7] (see e.g., Fig. 1):

$$E_W(A_1, A_2) = \mathrm{ext} \frac{\mathrm{Area}(\Sigma_{A_1 \cup A_2})}{4G_N}. \tag{1.2}$$

On the other hand, for large separations, the disconnected configuration is favored and the EWCS vanishes. Considering the above definition, different proposals that make connections between the EWCS and boundary correlation measures can be recapped as follows [6–9]:

*babaeivelni@guilan.ac.ir
†mmohammadi@guilan.ac.ir
‡vahidinia@iasbs.ac.ir

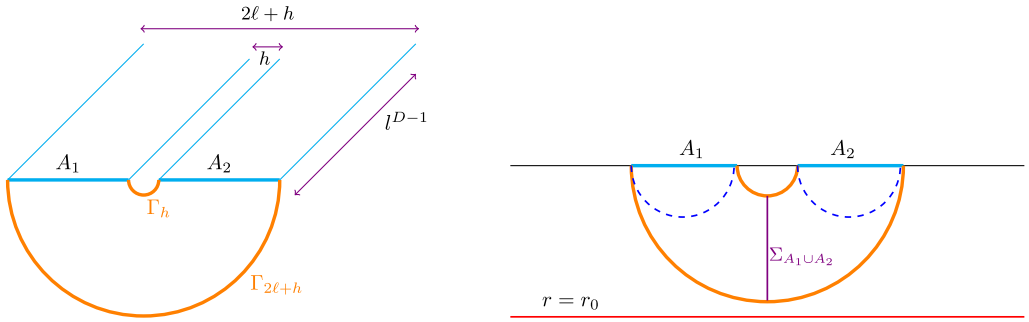

FIG. 1. Schematic configuration for computing HMI (left) and the EWCS (right). Here we just demonstrate the connected configuration where both the HMI and the EWCS are nonzero.

$$E_W(A_1, A_2) = E_P(A_1, A_2) = \frac{S_R(A_1, A_2)}{2} = S_O(A_1, A_2) - S(A_1 \cup A_2),$$

where E_P, S_R, and S_O are entanglement of purification, reflected entropy, and odd entropy respectively.[1] One may note that although they are not necessarily equivalent for a generic state, it seems they are the same for holographic states. Indeed, the EWCS may probe spacetime properties that are inaccessible from the perspective of holographic entanglement entropy (HEE). In particular, HEE is not a measure of quantum entanglement for a mixed state. This progress has motivated some interesting and extensive discussions of holographic correlation measures which have led to a remarkably rich and varied range of new insights in both holography and field theory, e.g., [12–42].

At the same time, there has been a great deal of interest in studying quantum quenches to understand whether and how quantum matter equilibrates. A prime arena for discussions of holographic quantum quench has been the Vaidya spacetime and this will also be the case in the present paper. This bulk geometry describes the gravitational collapse of a thin shell of matter to form a black hole which is dual to the evolution of a far from equilibrium initial state to a steady state in the boundary theory. Such shock-wave geometries have already been extensively studied in the context of holographic entanglement measures, e.g., [43–51]. It was argued in [46] that the evolution of EE can be captured by the picture of an entanglement tsunami, i.e., a wave propagating inward from the boundary of the entangled region. In this setup, one can derive in detail several universal features in the evolution of nonlocal measures in quenched holographic systems. In particular, for large entangling regions, the evolution of EE experiences different regimes of an early-time quadratic growth, an intermediate linear growth, and a late-time saturation. Further, employing the same picture, the nonequilibrium evolution of other measures such as mutual and tripartite information has been considered in [50,51]. Related studies attempting to better understand the evolution of entanglement measures in more general time-dependent bulk geometries have also appeared in [48,49].

In [52], we investigated the holographic proposals concerning the EWCS for Vaidya geometries describing a thin shell of null matter collapsing into the $(d+1)$-anti–de Sitter (AdS_{d+1}) vacuum to form a one-sided black brane. We considered a symmetric configuration consisting of two disjoint strips with equal width. A surprising result we found was that for large entangling regions, the evolution of the EWCS experiences the same scaling regimes as EE and the rate of growth of E_W is equal to S_A. In $2+1$ dimensions, we presented a combination of numerical and analytic results which support this behavior. Moreover, in higher-dimensional cases we provided a numerical treatment and examine the various regimes in the growth of the EWCS. Despite numerical results for the time dependence of this quantity, the question of full time evolution and in particular the rate of growth at intermediate times has not been thoroughly investigated. Hence, in the present paper, we employ an analytic treatment to study the full time evolution of EWCS in higher-dimensional Vaidya geometries. While this analysis can be done for a generic asymptotically AdS spacetime, in order to gain better insight into the properties of E_W, we generalize our study to specific nonrelativistic boundary theories, in particular, those with Lifshitz and hyperscaling violating exponents.

It is worthwhile to mention that as previously noted in [48,49], a nontrivial dynamical exponent can affect the rate of entanglement growth and hence the corresponding saturation time. We will confirm that (up to a time shift) the qualitative behavior of HEE and boundary measures dual to the EWCS is similar even in these nonconformal theories. Nevertheless, there are some challenges associated with studying holographic duality in nonrelativistic backgrounds, see e.g., [53,54]. In particular, the validity of HRT prescription and the ability to construct a well-defined

[1]Recently in [10] it was shown that S_R is not monotonically decreasing under partial trace, and so in general is not a measure of physical correlations. However, it seems that it is a valid correlation measure for holographic states as entanglement wedge nesting suggests [8,11].

entanglement wedge in the Lifshitz background is questionable [54]. In the present paper, we naively assume that the standard prescriptions for computing holographic entanglement entropy and the definition of the entanglement wedge are valid even in Lifshitz geometry.

This paper is structured as follows: In Sec. II we introduce the required preliminaries. We briefly review the Vaidya background with Lifshitz and hyperscaling violating exponents and then we carefully examine the general form of the EWCS functional in this geometry. Then, in Sec. III we study in detail the evolution of the EWCS in the formation of a black brane modeled by the time-dependent geometry for a null shell collapsing into the AdS vacuum spacetime. Throughout this section, we consider the large subregion limit, where analytic formulas for different information measures can be found. Afterwards, in Sec. IV we focus on the case where the boundary theory is nonrelativistic and we apply the same prescription to compute the evolution of the EWCS. We present an analytic derivation of the effect of Lifshitz and hyperscaling-violating exponents on entanglement velocity and the early and late-time behavior of the EWCS. Finally, we discuss some implications of our results, as well as possible future directions, in Sec. V.

II. SETUP

We are interested in the time evolution of the EWCS in the presence of an infalling thin null shell in a background with Lifshitz and hyperscaling-violating exponents. In this section, we review the background metric and then obtain the EWCS profile for two disjoint strip regions in the connected phase (see Fig. 1).

A. Vaidya geometry with Lifshitz and hyperscaling exponents

In this paper, we consider the following metric which describes collapsing of a null shell and the formation of a black brane in the vacuum background with Lifshitz scaling z and hyperscaling-violating exponent θ

$$ds^2 = r^{-2\frac{D-\theta}{D}}\left(-\frac{f(r,v)}{r^{2z-2}}\mathrm{d}v^2 - \frac{2}{r^{z-1}}\mathrm{d}v\,\mathrm{d}r + \mathrm{d}\mathbf{x}_D^2\right),$$
$$f(r,v) = \begin{cases} 1 & v<0 \\ g(r) & v>0 \end{cases}, \qquad g(r) = 1-\left(\frac{r}{r_0}\right)^{D-\theta+z}, \tag{2.1}$$

where we employ the Eddington-Finkelstein-like coordinate, i.e., $\mathrm{d}v = \mathrm{d}t - r^{z-1}\frac{\mathrm{d}r}{f}$. One may note that inside the shell ($v<0$) the spacetime is given by hyperscaling-violation Lifshitz (HSL) metric while the outside region ($v>0$) is an asymptotically HSL black brane. As we mentioned it may model a sort of global quench in the dual boundary theory. This metric reduces to the relativistic AdS-Vaidya geometry for $z=1$ and $\theta=0$. We assume that this Vaidya-type metric is a solution to Einstein's theory with some suitable matter fields. For example, it was shown that the Einstein-Maxwell-dilaton theory admits such solution [55]

$$\mathcal{I} = -\frac{1}{16\pi G_N}\int \mathrm{d}^{D+2}x\left[R - \frac{1}{2}(\partial\phi)^2 + V_0 e^{\gamma\phi} - \frac{1}{4}\sum_i^2 e^{\lambda_i\phi}F_i^2\right]. \tag{2.2}$$

It is appropriate to define an effective dimension

$$d := D-\theta+1$$

that for $\theta=0$ reduces to the dimension of dual boundary QFT$_d$.

At late times, the bulk metric (2.1) describes a black brane with a horizon at r_0. The temperature, thermal entropy density associated with the horizon, and energy density [56] are

$$T = \frac{d+z-1}{4\pi r_0^z}, \qquad \mathcal{S}_{\mathrm{th}} = \frac{1}{4G_N}\frac{1}{r_0^{d-1}}, \qquad \mathcal{E} = \frac{d-1}{16\pi G_N}\frac{1}{r_0^{d+z-1}}. \tag{2.3}$$

In what follows we assume that $z\geq 1$ and $d>1$. It ensures that the null energy condition is satisfied and the black-brane solution is thermodynamically stable. Also in this case the zero-temperature entanglement entropy is consistent with the previous results [57].

B. EWCS in Vaidya background

We are interested in the time evolution of the EWCS associated with two identical long strips (A_1 and A_2) on the boundary (see Fig. 1). We will take them to be of width ℓ, length l and are separated by distant h. The EWCS is given by Eq. (1.2) and we assume that $h \ll \ell$, ensures the entanglement wedge is connected and the EWCS does not vanish. In this configuration, the entanglement wedge is bounded by two extremal hypersurfaces anchored to boundary strips with size $2\ell+h$ and h. In Fig. 1 we denote these hypersurfaces by $\Gamma_{2\ell+h}$ and Γ_h, respectively. Moreover, we denote the turning points of $\Gamma_{2\ell+h}$ and Γ_h by r_u and r_d respectively. The EWCS can be parametrized as $v=v(r)$ and due to the reflection symmetry about $x=0$ the induced metric on $\Sigma_{A_1\cup A_2}$ simplified as follows:

$$ds^2_{\mathrm{ind}} = r^{\frac{-2(D-\theta)}{D}}\left[-\left(f(r,v)v'^2 + 2r^{z-1}v'\right)\frac{\mathrm{d}r^2}{r^{2z-2}} + \mathrm{d}\mathbf{x}^2_{D-1}\right]. \tag{2.4}$$

Now using Eq. (1.2) the E_W which is proportional to the extremal area of the corresponding codimension-2 hypersurface is given by the following functional

$$E_W = \frac{l^{D-1}}{4G_N}\int \mathrm{d}r \frac{\mathscr{E}}{r^{d-1}}, \qquad \mathscr{E} \coloneqq \sqrt{-\frac{2v'}{r^{z-1}} - \frac{f(r,v)v'^2}{r^{2z-2}}}. \tag{2.5}$$

Extremizing the above expression yields the equation of motion for $v(r)$

$$\frac{\partial}{\partial r}\left(\frac{r^{z-1}+f(r,v)v'}{r^{d+2z-3}\mathscr{E}}\right) = \frac{v'^2}{2r^{d+2z-3}\mathscr{E}}\frac{\partial f}{\partial v}. \tag{2.6}$$

To obtain the extremal hypersurface we need to solve the above equation by assuming certain boundary conditions

$$v(r_d) = v_d, \qquad v(r_u) = v_u, \tag{2.7}$$

where r_d and r_u are the turning points of hypersurfaces Γ_h and $\Gamma_{h+2\ell}$, respectively. Note that for $v \neq 0$, $\frac{\partial f}{\partial v} = 0$ and we have a conserved quantity as follows:

$$\frac{r^{z-1}+f(r,v)v'}{r^{d+2z-3}\mathscr{E}} = \frac{\mathcal{Q}}{r_0^{d+z-2}}. \tag{2.8}$$

Using this fact, we can solve Eq. (2.6) for $v'(r)$ to get

$$v'_{\pm} = -\frac{r^{z-1}}{f}\left(1 \mp \frac{\mathcal{Q}(r/r_0)^{d+z-2}}{\mathcal{A}}\right),$$
$$\mathcal{A} \coloneqq \sqrt{f + \mathcal{Q}^2(r/r_0)^{2(d+z-2)}}. \tag{2.9}$$

One may note that $\mathcal{Q} \to -\mathcal{Q}$ implies $v_{\pm} \to v_{\mp}$, so in what follows without loss of generality, we only consider the v_- branch. Discontinuity of $f(r,v)$ requires studying $\mathcal{Q}$ in the HSL region ($v < 0$) and black-brane region ($v > 0$) separately and then matching the results at the point where the null shell and the EWCS intersect. Note that in the following we will use the subscripts a and b to refer to quantities on the HSL and black-brane side, respectively.

1. HSL region ($v < 0$)

In this case $f(r,v) = 1$ and Eq. (2.9) reduces to

$$v'_- = -r^{z-1}\left(1 + \frac{\mathcal{Q}_- r^{d+z-2}}{\mathcal{A}_-}\right), \tag{2.10}$$

where $\mathcal{Q}_- r_0^{d+z-2} \coloneqq \mathcal{Q}$ and $\mathcal{A}_- \coloneqq \mathcal{A}(\mathcal{Q}_- r_0^{d+z-2}, r)|_{f=1}$. Therefore, the profile of the EWCS becomes

$$v_-(r) = c_- - \frac{r^z}{z} - \mathcal{F}(r), \tag{2.11}$$

where

$$\mathcal{F}(r) \coloneqq \int^r \frac{\mathcal{Q}_- r'^{d+2z-3}\mathrm{d}r'}{\mathcal{A}_-} = \frac{r^z}{z}\,{}_2F_1\left(\frac{1}{2}, \ell, 1+\ell, -\frac{r^{z/\ell}}{\mathcal{Q}_-^2}\right), \tag{2.12}$$

and $\ell \coloneqq \frac{z}{2(2-d-z)}$. By imposing the boundary condition $v_-(r_u) = v_u$ we can fix the integration constant as

$$c_- = v_u + \frac{r_u^z}{z} + \mathcal{F}(r_u). \tag{2.13}$$

Note that for $d = 2$ and $z = 1$ the above expressions precisely match with the previous results reported in [52].

2. Black-brane region ($v > 0$)

Now, let us consider the profile in the black-brane region where $f(r,v) = g(r)$. In this case using Eq. (2.9), one derives the profile of EWCS in $v > 0$ region as follows:

$$v_+(r) = c_+ - \mathcal{G}(r) - \mathcal{Q}_+ r_0^z \int_{\frac{r_d}{r_0}}^{\frac{r}{r_0}} \mathrm{d}u \frac{u^{d+2z-3}}{g(u)\mathcal{A}_+}, \qquad u \coloneqq \frac{r}{r_0}, \tag{2.14}$$

where $\mathcal{A}_+ = \mathcal{A}(\mathcal{Q}_+, r)|_{f=g}$ and $\mathcal{G}$ is defined as

$$\mathcal{G}(r) \coloneqq \int \frac{\mathrm{d}r}{g(r)} = r\,{}_2F_1\left(1, \bar{\ell}, 1+\bar{\ell}, \left(\frac{r}{r_0}\right)^{1/\bar{\ell}}\right), \tag{2.15}$$

where $\bar{\ell} \coloneqq \frac{1}{d+z-1}$. Once again using the boundary condition $v_+(r_d) = v_d$ one can obtain the integration constant

$$c_+ = v_d + \mathcal{G}(r_d). \tag{2.16}$$

3. Matching at $v = 0$

By integrating Eq. (2.6) across the null shell at $v(r_w) = 0$, we obtain the corresponding matching condition

$$\left.\frac{\mathrm{d}r}{\mathrm{d}v}\right|_- - \left.\frac{\mathrm{d}r}{\mathrm{d}v}\right|_+ = -\frac{1}{2}\left(\frac{r_w^d}{r_0^{d+z-1}}\right). \tag{2.17}$$

Solving the above condition, we get the relation between the conserved quantities, i.e., $\mathcal{Q}_-$ and $\mathcal{Q}_+$ as follows:

$$\mathcal{Q}_+ = \pm\frac{\left(r_w^{d+z-1} - 2r_0^{d+z-1}\right)\mathcal{Q}_- + r_w\mathcal{A}_-(r_w)}{2r_0}. \tag{2.18}$$

Without loss of generality in the rest of the paper, we take the positive sign. On the other hand, the continuity of the EWCS profile at the intersection point, i.e., $v_a(r_w) = 0 = v_b(r_w)$ implies

$$v_u + \frac{r_u^z}{z} + \mathcal{F}(r_u) - \frac{r_w^z}{z} - \mathcal{F}(r_w) = 0, \tag{2.19a}$$

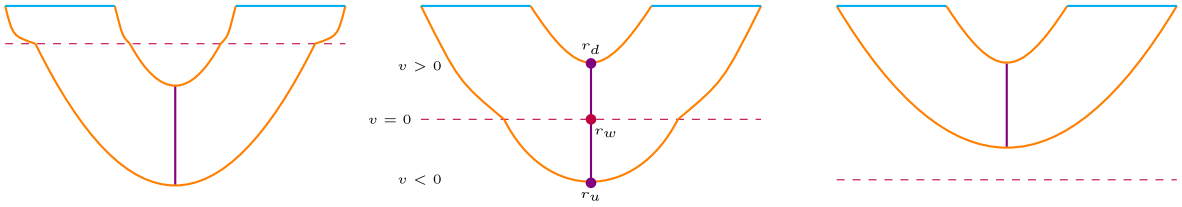

FIG. 2. Schematic configurations for HRT and EWCS hypersurfaces corresponding to the connected phase where the separation between the boundary entangling regions is small. Outside the collapsing shell (indicated in dashed purple), i.e., $v > 0$, the hypersurfaces propagate in an AdS black-brane spacetime. On the other hand, in $v < 0$ region, they propagate in a pure AdS geometry. *Left*: At early times the null shell lies near the boundary of the spacetime and Σ does not intersect the shell. *Middle*: During intermediate stages of evolution Σ crosses the null shell. *Right*: At the late-time Σ lies entirely in black-brane geometry.

$$v_d + \mathcal{G}(r_d) - \mathcal{G}(r_w) - \mathcal{Q}_+ r_0^z \int_{\frac{r_d}{r_0}}^{\frac{r}{r_0}} \mathrm{d}u \, \frac{u^{d+2z-3}}{g(u)\mathcal{A}_+} = 0. \quad (2.19b)$$

Note that when r_d is located in the black-brane region where $v_d > 0$ one can use $\mathrm{d}t = \mathrm{d}v + r^{z-1}\frac{\mathrm{d}r}{g}$ and $t = v_d + \mathcal{G}(r_d)$ to express the boundary time in terms of other parameters as follows:

$$t = \mathcal{G}(r_w) + \mathcal{Q}_+ r_0^z \int_{\frac{r_d}{r_0}}^{\frac{r_w}{r_0}} \mathrm{d}u \, \frac{u^{d+2z-3}}{g(u)\mathcal{A}_+}. \quad (2.20)$$

These conditions are sufficient to obtain the EWCS in terms of v_u, v_d, as well as r_w which are related to the boundary parameters ℓ, h, and t, respectively. So in principle, by using them one may obtain the contribution to the EWCS in both regions

$$\tilde{E}_W^- = \int_{r_w}^{r_u} \frac{r^{1-d}\mathrm{d}r}{\mathcal{A}_-}, \quad (2.21a)$$

$$\tilde{E}_W^+ = \frac{1}{r_0^{d-2}} \int_{\frac{r_d}{r_0}}^{\frac{r_w}{r_0}} \frac{u^{1-d}\mathrm{d}u}{\mathcal{A}_+}, \quad (2.21b)$$

where we have defined $E_W := \frac{l^{D-1}}{4G_N}\tilde{E}_W$ for simplicity. Finally using these equations we can read E_W as

$$E_W = E_W^- + E_W^+. \quad (2.22)$$

In the next sections following [58], we will study the time evolution of E_W in three different scaling regimes. Before we proceed further, let us comment on an assumption that greatly simplifies the calculation.

C. Notes on $\mathcal{Q}_-$ and $\mathcal{Q}_+$

In what follows we mainly consider a specific limit where the characteristic size of the boundary entangling regions is large compared to the inverse temperature, i.e., $\ell T^{1/z} \gg hT^{1/z} \gg 1$. Indeed, we will argue that $\mathcal{Q}_- \approx 0$ in this limit. It leads to a great simplification in the semianalytic results for E_W. To show this, first, note the relation between r_w and r_c. These quantities indicate positions where the null shell intersects $\Sigma_{A_1 \cup A_2}$ and $\Gamma_{2\ell+h}$, respectively (see Fig. 2). It is easy to show that $r_c^z = zv_u + r_u^z$ which simplifies Eq. (2.19a) as follows:

$$r_w^z - r_c^z = z\mathcal{F}(r_u) - z\mathcal{F}(r_w).$$

Note that the null shell intersects the EWCS at r_w and in general $r_w \neq r_c$ but one may expect that $r_c \approx r_w$. Indeed, our numerical results confirm this expectation see, e.g., Fig. 3. Based on this figure, when the connected configuration is always favored for any boundary time, these quantities precisely match at early and intermediate times. On the other hand, when the disconnected configuration is favored at late times, although at early times r_c matches with r_w, the deviation between them becomes more pronounced as time evolves. Further, by expanding the hypergeometric function in Eq. (2.12), it is easy to show that

$$\frac{r_w^z}{z} - \frac{r_c^z}{z} = \sum_{n=0}^{\infty} \mathcal{C}_n^{-\frac{1}{2}} \frac{r_u^{p_n} - r_w^{p_n}}{p_n} \mathcal{Q}_-^{2n+1},$$
$$p_n = 2n(d-1) + d + 2(z-1)(n+1), \quad (2.23)$$

where $\mathcal{C}_n^{-\frac{1}{2}} = \Gamma(1/2)/\Gamma(n+1)\Gamma(1/2-n)$. So for $r_c \approx r_w \ll r_u$ this equation requires $\mathcal{Q}_- \to 0$. Then from Eq. (2.18) we get

$$\mathcal{Q}_- \approx 0 \quad \text{and} \quad \mathcal{Q}_+ \approx -\frac{r_w}{2r_0}, \qquad (r_w \ll r_u). \quad (2.24)$$

In the following sections, we will employ these relations to study the scaling of E_W during the early and intermediate stages of time evolution.

However, when $r_w \approx r_u$, we cannot assume $\mathcal{Q}_- = 0$. Indeed, in this situation, $\mathcal{Q}_+ \approx 0$ and $\mathcal{Q}_- \neq 0$. To see this, note that as $r_w \to r_u$ the $\Gamma_{2\ell+h}$ settles down to its final static configuration as it lies in the black-brane geometry and hence $t \approx v_u + \mathcal{G}(r_u)$. On the other hand, the latter should be consistent with Eq. (2.20) upon substituting $r_w \approx r_u$

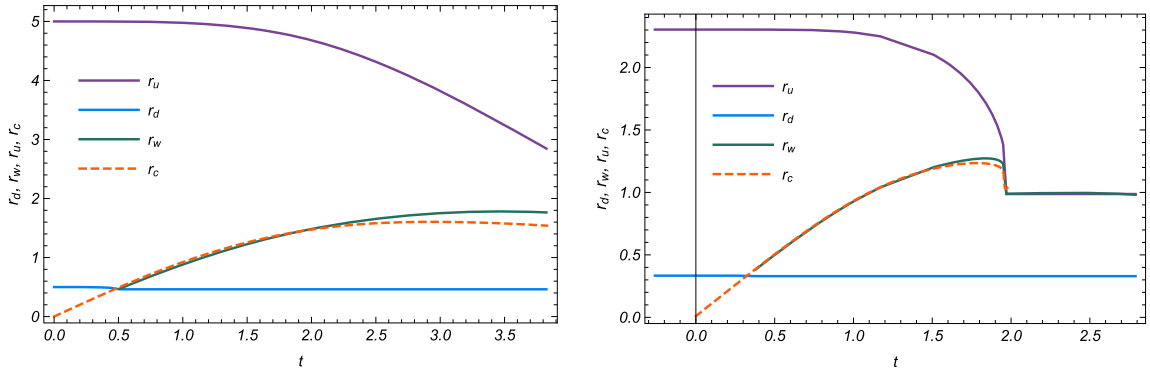

FIG. 3. Time evolution of r_d, r_u, r_w, and r_c for $z = 1$. Clearly, at the early time we have $r_w \approx r_c$ and the deviation between them becomes more pronounced near the saturation time. *Left:* $d = 2$, $h = 1$, and $\ell = 4.5$. *Right:* $d = 3$, $h = 0.4$, and $\ell = 1.18$. Here we set $r_0 = 1$.

$$v_u + \mathcal{G}(r_u) = \mathcal{G}(r_u) + \mathcal{Q}_+ r_0^z \int_{\frac{r_d}{r_0}}^{\frac{r_u}{r_0}} \mathrm{d}u \frac{u^{d+2z-3}}{g(u)\mathcal{A}_+}. \tag{2.25}$$

Now, we note that $v_u = v(r_u \to r_w) \approx 0$ and then the above equation implies $\mathcal{Q}_+ \to 0$. In this situation, by solving Eq. (2.18) for $\mathcal{Q}_+ = 0$ one obtains

$$\mathcal{Q}_-^2 \approx \frac{r_u^2}{4r_0^{d+z-1}\left(r_0^{d+z-1} - r_u^{d+z-1}\right)}, \quad \text{and}$$
$$\mathcal{Q}_+ \approx 0, \qquad (r_w \approx r_u). \tag{2.26}$$

As we will argue, this result allows us to explore the saturation of E_W as the EWCS lies entirely in the black-brane region.

III. EWCS IN AdS BLACK BRANE ($z = 1, \theta = 0, d > 2$)

We shall now discuss the time evolution of the EWCS in the various regimes with a collapsing shell of matter in asymptotic AdS spacetime which describes a relativistic quantum quench. As we explained in the previous section, we are interested in the connected configuration where EWCS is nontrivial. We also focus on the regime where the null shell intersects the EWCS (see Fig. 2). In such circumstances, we investigate three different regimes: (i) *Early growth* describes the behavior of E_W immediately after the null shell passes through the r_d. So in this regime, we should assume $r_d \lesssim r_w$; (ii) *Linear growth* characterizes situation where $r_u \gg r_w \gg r_d$; (iii) *Saturation* which shows how the E_W reaches to its equilibrium value.

We remind the reader that a similar study for $d = 2$ has been done in [52], thus here we just focus on $d \geq 3$. Moreover, in the next section, we discuss the effects of z and θ on the EWCS evolution by exploring the HSL background.

A. Early growth

As we just mentioned, the collapsing shell does not intersect Σ at very early time (see Fig. 2). Although, the entanglement entropy starts its early growth during this period of time [58], the EWCS does not change and is given by E_W^-. So here, by early growth, we mean the time evolution of the EWCS right after the null shell intersects Σ. To compute the time dependence of E_W at early time, we suppose $r_d \lesssim r_w$ and $r_d \ll r_0 \ll r_u$. It allows us to consider $r_w = r_d + \delta$ where $\delta \ll r_d \ll r_0$. Moreover, the large interval $r_0 \ll r_u$ lets to use Eq. (2.24) in order to expand Eq. (2.21b) up to the first order that depends on r_0

$$\tilde{E}_W^+ = \frac{\delta}{r_d^{d-1}} - \frac{(d-1)}{2}\frac{\delta^2}{r_d^d} + \frac{\delta^2 + 2r_d\delta}{4r_0^d} + \mathcal{O}\left(\frac{\delta^3}{r_d^{d+1}}, \frac{\delta r_d^{d+1}}{r_0^{2d}}\right). \tag{3.1}$$

On the other hand, we may obtain E_W^- piece by applying $\mathcal{Q}_- = 0$ in Eq. (2.21a)

$$\tilde{E}_W^- = \frac{1}{(d-2)r_w^{d-2}} - \frac{1}{(d-2)r_u^{d-2}} + \mathcal{O}\left(\mathcal{Q}_-^{\frac{d-2}{d-1}}\right). \tag{3.2}$$

Further, Eq. (3.1) suggests that one should expand E_W^- around $r_w = r_d + \delta$ up to $\mathcal{O}(\delta^3)$

$$\tilde{E}_W^- = \frac{1}{(d-2)r_d^{d-2}} - \frac{1}{(d-2)r_u^{d-2}} - \frac{\delta}{r_d^{d-1}} + \frac{(d-1)}{2}\frac{\delta^2}{r_d^d} + \mathcal{O}(\delta^3) + \mathcal{O}\left(\mathcal{Q}_-^{\frac{d-2}{d-1}}\right). \tag{3.3}$$

Now we are equipped with all we need to calculate the early growth of the EWCS in terms of δ as follows:

$$\tilde{E}_W = \frac{1}{(d-2)r_d^{d-2}} - \frac{1}{(d-2)r_u^{d-2}} + \frac{\delta^2 + 2r_d\delta}{4r_0^d} + \mathcal{O}(\delta^3, r_d^d). \tag{3.4}$$

However, we are interested in the explicit dependence of the EWCS on boundary time. Therefore we expand Eq. (2.20) to get δ in the terms of t

$$t = \delta + r_d + \mathcal{O}(r_d^d, r_d^{d-1}\delta^2). \tag{3.5}$$

Substituting the above result into Eq. (3.4) we obtain the time scaling of E_W in this regime as

$$\tilde{E}_W \approx \tilde{E}_W^-(r_d, r_u) + \frac{t^2 - r_d^2}{4r_0^d}. \tag{3.6}$$

The first term describes the $\tilde{E}_W$ in the static AdS space and so one may call it the vacuum contribution. By subtracting it we obtain one of our main results

$$\Delta E_W \approx \frac{\pi l^{d-2}\mathcal{E}}{d-1}\left(t^2 - \frac{h^2}{c^2}\right), \tag{3.7}$$

where the energy density of the boundary state $\mathcal{E}$ is defined in Eq. (2.3). We also use $h \approx c r_d$ to fully express the final result in terms of the boundary quantities.[2] The above result shows that the early growth of E_W starts at $t \sim h$, in contrast to entanglement entropy where its early growth begins at $t = 0$. Moreover, as one may expect, for $h \to 0$ this result matches with the early growth of entanglement entropy [58].

B. Linear growth and saturation

Here we survey regime corresponds to $h \ll r_0 \ll t \ll \ell$ where $r_w \ll r_u$. First, let us recall Eqs. (2.21b) and (2.20) as

$$\tilde{E}_W^+ = \frac{1}{r_0^{d-2}}\int_{\frac{r_d}{r_0}}^{\frac{r_w}{r_0}} \frac{u^{1-d}\mathrm{d}u}{\mathcal{A}_+(u, u_w)},$$
$$t = \mathcal{G}(r_w) + \mathcal{Q}_+ r_0 \int_{\frac{r_d}{r_0}}^{\frac{r_w}{r_0}} \frac{u^{d-1}\mathrm{d}u}{g(u)\mathcal{A}_+(u, u_w)}, \tag{3.9}$$

where $\mathcal{A}_+$ depends on u_w via Eq. (2.18). Now let us suppose that there is a minimum for $\mathcal{A}_+$ at $\boldsymbol{u}_\mathrm{m}$ and so $\partial_u \mathcal{A}_+(u)|_{\boldsymbol{u}_\mathrm{m}} = 0$. Moreover, we also assume that at $u = \boldsymbol{u}_\mathrm{m}$ there is a $u_w = \boldsymbol{u}_\star$ such that $\mathcal{A}_+(\boldsymbol{u}_\mathrm{m}, \boldsymbol{u}_\star) = 0$. Indeed, our numerical results confirm these assumptions see e.g., Fig. 4. Based on this figure, we see that during the evolution, r_w approaches $r_w^\star$ corresponds to the linear-growth regime.

[2]For $r_d \ll r_0$ (low temperature limit $hT^{1/z} \ll 1$)

$$r_d \approx \frac{h}{c}\left(1 - \frac{\sqrt{\pi}}{(d+z)c^{d+z}}\frac{\Gamma\left(\frac{2d+z-1}{2(d-1)}\right)}{\Gamma\left(\frac{d+z}{2(d-1)}\right)}\left(\frac{h}{r_0}\right)^{d+z-1}\right),$$
$$c = \frac{2\sqrt{\pi}\Gamma\left(\frac{d}{2(d-1)}\right)}{\Gamma\left(\frac{1}{2(d-1)}\right)}. \tag{3.8}$$

In this plot, we consider the values of ℓ and h such that the disconnected configuration is favored at late times. Hence the saturation is discontinuous and the corresponding extremal hypersurface jumps at some saturation time where each curve stops. Moreover, it is clear that, as ℓ increases, also the linear regime increases. Based on these observations the dominant part of the integrals in Eq. (3.9) comes from the region near $\boldsymbol{u}_\mathrm{m}$ and $\boldsymbol{u}_\star$. It is similar to what happens in the time evolution of HEE as discussed in [58]. Existence of $\boldsymbol{u}_\star$ implies $\mathcal{Q}_+^\star = \mathcal{Q}_+|_{\boldsymbol{u}_\star}$. Thus, by expanding $\mathcal{A}_+$ about $u = \boldsymbol{u}_\mathrm{m}$ and $\boldsymbol{u}_\star$ (or $\mathcal{Q}_+$), we get

$$\mathcal{A}_+ \approx c_1(u - \boldsymbol{u}_\mathrm{m})^2 + c_2(\mathcal{Q}_+^\star - \mathcal{Q}_+), \tag{3.10}$$

where

$$c_1 := \frac{1}{2}\partial_u^2 \mathcal{A}_+|_{\boldsymbol{u}_\mathrm{m}, \boldsymbol{u}_\star}, \qquad c_2 := -\partial_{\mathcal{Q}_+}\mathcal{A}_+|_{\boldsymbol{u}_\mathrm{m}, \boldsymbol{u}_\star},$$
$$\mathcal{Q}_+^\star := \boldsymbol{u}_\mathrm{m}\frac{\sqrt{(d-2)d}}{2(d-1)}, \qquad \boldsymbol{u}_\mathrm{m} := \left(\frac{2(d-1)}{d-2}\right)^{1/d}.$$

Using Eq. (3.10) we estimate the integral of E_W as

$$\tilde{E}_W^+ = \frac{{\boldsymbol{u}_\mathrm{m}}^{1-d}}{r_0^{d-2}}\int_{\frac{r_d}{r_0}}^{\frac{r_w}{r_0}} \frac{\mathrm{d}u}{\mathcal{A}_+}. \tag{3.11}$$

On the other hand, inserting Eq. (3.10) in Eq. (3.9) and simplify the resultant equation yields

$$t - t_\star \approx \frac{\mathcal{Q}_+^\star r_0 {\boldsymbol{u}_\mathrm{m}}^{d-1}}{g(\boldsymbol{u}_\mathrm{m})}\int_{\frac{r_d}{r_0}}^{\frac{r_w}{r_0}} \frac{\mathrm{d}u}{\mathcal{A}_+}, \tag{3.12}$$

where $t_\star := \mathcal{G}(r_w^\star)$. The above results imply the linear growth of E_W in this regime

$$\Delta E_W \approx l^{d-2}\mathcal{S}_\mathrm{th} V_W (t - t_\star), \tag{3.13}$$

where $\Delta E_W = E_W - E_W^-(r_w^\star, r_u)$ and then the velocity V_W is given by

$$V_W := \frac{g(\boldsymbol{u}_\mathrm{m})}{\mathcal{Q}_+^\star {\boldsymbol{u}_\mathrm{m}}^{2d-2}} = \left(\frac{d-2}{2(d-1)}\right)^{\frac{d-1}{d}}\sqrt{\frac{d}{d-2}}. \tag{3.14}$$

One may note that the linear behavior is similar to the growth of entanglement entropy. In addition, the expression for V_W is the same as the entanglement velocity defined in [58].

As the null shell approaches the turning point r_u, the EWCS falls into the balk brane region. So the value of E_W should reduce to that in the static black-brane geometry. In other words, the EWCS saturates its equilibrium value which is the same as E_W at the thermal state. To see this, note that Eq. (2.21a) shows $E_W^- \to 0$ as $r_w \to r_u$. In addition, we recall Eq. (2.26) in this regime and by

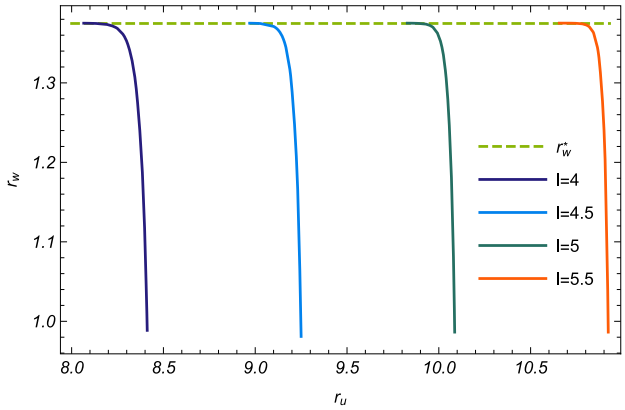

FIG. 4. $(r_w(t), r_u(t))$ for different values of ℓ with $h = 2.1$ and $z = 1$. During the evolution, r_w approaches $r_w^\star$ corresponds to the linear-growth regime. For these values of ℓ and h the disconnected configuration is favored at late times and the extremal hypersurface jumps at some saturation time where each curve stops. Here we set $r_0 = 1$.

employing $\mathcal{Q}_+ = 0$ in Eq. (2.21b) we get the E_W for the black-brane geometry [13]

$$E_W = \frac{l^{D-1}}{4G_N}\int_{r_d}^{r_u}\frac{r^{1-d}\mathrm{d}r}{\sqrt{g(r)}}. \tag{3.15}$$

It is worthwhile mentioning that the above analysis works when the connected configuration is always favored for any boundary time during the thermalization and the resultant E_W continuously saturates to the final equilibrium value given by Eq. (3.15). However, we should also remark that when the disconnected configuration is favored, the late-time behavior of the EWCS changes such that it displays a discontinuous transition and immediately saturates to zero.

IV. EWCS IN HLS BLACK BRANE ($z \neq 1$, $\theta \neq 0$)

In this section, we generalize our studies to holographic theories with general dynamical critical exponent z and hyperscaling violation exponent θ. Employing the analysis we have outlined in the previous section we will be able to explore a variety of scaling regimes in the time evolution of EWCS. As we will see its behavior is qualitatively similar to HEE previously discussed in [48,49].

A. Early growth

As we explain in the previous section for $z = 1$, at early times we expect that $r_w \approx r_c$. Indeed, our numerical results show that this behavior holds even in the nonrelativistic case, see e.g., Fig. 5. In this case, r_w always coincides with r_c for any boundary time. Interestingly, comparing these results with the results depicted in Fig. 3, we see that r_w and r_c will be in complete agreement if we choose larger values of z. Recall that at early times, i.e., $t \ll r_0^z$, the shell does not reach Σ which lies entirely in HLS geometry, and thus the EWCS is a fixed constant given by the vacuum value. Let us start from Eq. (2.21a) and expand it up to the first term that depends on r_0

$$\tilde{E}_W^+ \approx \frac{1}{(d-2)r_d^{d-2}} - \sum_{n=0}^{z+1}\frac{\mathcal{C}_n^{2-d}}{d-2}\frac{\delta^n}{r_d^{d+n-2}} + \frac{(r_d+\delta)^{z+1} - r_d^{z+1}}{2(z+1)r_0^{d+z-1}}, \tag{4.1}$$

where $\mathcal{C}_n^m$ denotes the binomial coefficient. It suggests that one should expand Eq. (2.21b) around $r_w = r_d + \delta$ up to $\mathcal{O}(\delta^{z+2})$

$$\tilde{E}_W^- \approx \sum_{n=0}^{z+1}\frac{C_n^{2-d}}{d-2}\frac{\delta^n}{r_d^{d+n-2}} - \frac{1}{(d-2)r_u^{d-2}}. \tag{4.2}$$

Now, using $\tilde{E}_W = \tilde{E}_W^- + \tilde{E}_W^+$ we get

$$\tilde{E}_W \approx \tilde{E}_W^-(r_d, r_u) + \frac{(r_d+\delta)^{z+1} - r_d^{z+1}}{2(z+1)r_0^{d+z-1}}. \tag{4.3}$$

To obtain δ as a function of time we employ Eq. (2.20) for $\{r_d, r_w\} \ll \{r_u, r_0\}$ and assume $r_w = r_d + \delta$ to read

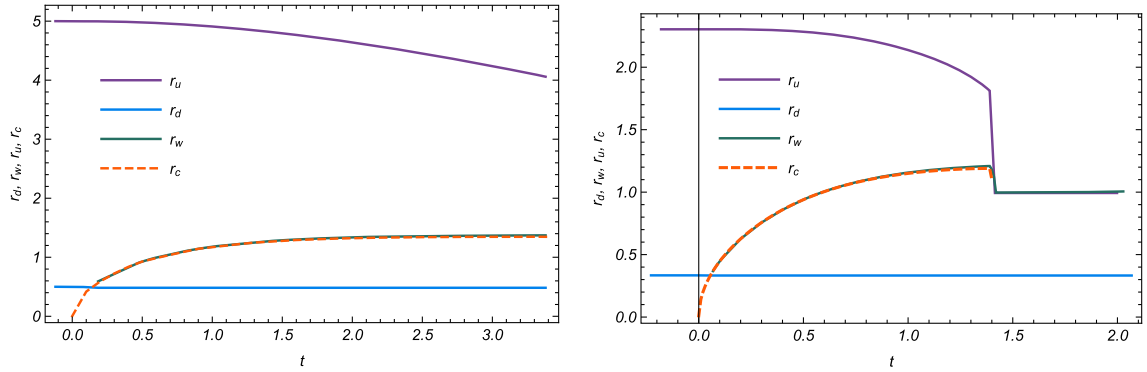

FIG. 5. Evolution of r_d, r_u, r_w and r_c for $z = 2$. Clearly, r_w always coincides with r_c for any boundary time. *Left:* $d = 2$, $h = 1$, and $\ell = 4.5$. *Right:* $d = 3$, $h = 0.4$, and $\ell = 1.18$. Here we set $r_0 = 1$.

$$\delta \approx (zt)^{\frac{1}{z}} - r_d. \tag{4.4}$$

It allows us to express the time evolution as

$$\Delta E_W \approx \frac{2\pi l^{D-1}\mathcal{E}}{(d-1)(z+1)}\left((zt)^{1+\frac{1}{z}} - \left(\frac{h}{\mathscr{c}}\right)^{z+1}\right), \tag{4.5}$$

where $\mathscr{c}$ is defined in Eq. (3.8). For $z=1$, this result reduces to that for Vaidya-AdS Eq. (3.7). Moreover, one may note that the scaling at the early time just depends on the Lifshitz exponent z and is independent of the hyperscaling-violating exponent θ. It is worth noting that in $h \to 0$ limit, it reduces to HEE [48,49].

B. Linear growth and saturation

Here we follow the same steps as in Sec. III B to figure out time scaling of EWCS for $h \ll r_0 \ll t^{1/z} \ll \ell$ where $\{r_w, r_c\} \ll r_u$. Again, in the presence of θ and z we consider $\mathcal{A}_+$ that has a minimum at $\boldsymbol{u}_{\rm m}$ and $\mathcal{A}(\boldsymbol{u}_{\rm m}, \boldsymbol{u}_\star) = 0$. Our numerical results confirm these assumptions see e.g., Fig. 6. We see that during the evolution, r_w approaches $r_w^\star$ in the linear-growth regime. Using the same expansion as Eq. (3.10) one finds

$$\begin{aligned}\boldsymbol{u}_{\rm m} &= \left(\frac{(d+z-2)}{d+z-3}\right)^{\frac{1}{d+z-1}},\\ \mathcal{Q}_+^\star &= -\boldsymbol{u}_{\rm m}\frac{\sqrt{(d+z-3)(d+z-1)}}{2(d+z-2)}.\end{aligned} \tag{4.6}$$

Once again, these assumptions simplify expressions for E_W^+ and $t - t_\star$ as follows:

$$\begin{aligned}E_W^+ &\approx \frac{2l^{D-1}r_0}{\boldsymbol{u}_{\rm m}{}^{d-1}}\mathcal{S}_{\rm th}\int_{\frac{r_d}{r_0}}^{\frac{r_w}{r_0}}\frac{\mathrm{d}u}{\mathcal{A}_+},\\ t - t_\star &\approx \frac{\mathcal{Q}_+^\star r_0^z \boldsymbol{u}_{\rm m}{}^{d+2z-3}}{g(\boldsymbol{u}_{\rm m})}\int_{\frac{r_d}{r_0}}^{\frac{r_w}{r_0}}\frac{\mathrm{d}u}{\mathcal{A}_+}.\end{aligned} \tag{4.7}$$

Now combining the above two equations yields the following:

$$\Delta E_W \approx l^{D-1}\mathcal{S}_{\rm th}\frac{2g(\boldsymbol{u}_{\rm m})}{\mathcal{Q}_+^\star \boldsymbol{u}_{\rm m}{}^{2d+2z-4} r_0^{z-1}}(t - t_\star). \tag{4.8}$$

Expressing this formula in terms of the boundary quantities yields

$$\Delta E_W \approx l^{D-1}\mathcal{S}_{\rm th} V_W (t - t_\star), \tag{4.9}$$

where the velocity of the linear growth depends on both z and θ (via $d = D - \theta + 1$) as follows:

$$V_W = \left(\frac{4\pi T}{d+z-1}\right)^{\frac{z-1}{z}}\left(\frac{d+z-3}{2(d+z-2)}\right)^{\frac{d+z-2}{d+z-1}}\sqrt{\frac{d+z-1}{d+z-3}}. \tag{4.10}$$

We note that for $z \neq 1$ the above velocity depends on the temperature of the final equilibrium state. Interestingly it is just the velocity of the linear growth for entanglement entropy in the presence of Lifshitz and hyperscaling-violating exponents [48,49]. Indeed, in these references the final result for HEE in the linear growth regime was written in terms of the horizon radius [similar to Eq. (4.8)], thus the first factor in Eq. (4.10) was neglected.

C. Saturation

As we explained in the previous section for the relativistic case, when the null shell reaches the turning point of $\Gamma_{2\ell+h}$, the EWCS in the nonrelativistic background also saturates its equilibrium value. As far as the connected configuration is favored, the resultant value of E_W is given by Eq. (3.15) while for a disconnected configuration, it vanishes abruptly. In Fig. 7 we show the evolution of

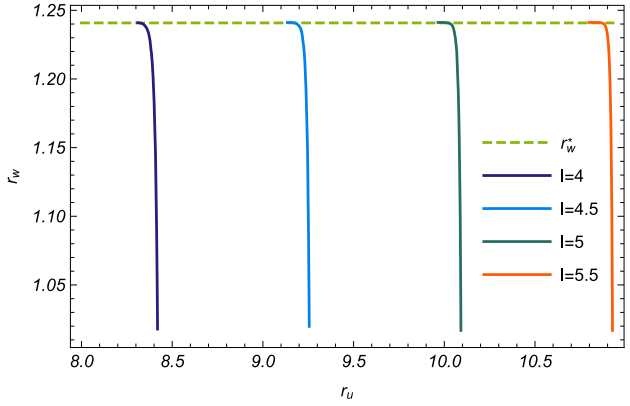

FIG. 6. $(r_w(t), r_u(t))$ for different values of ℓ with $h = 2.1$ and $z = 2$. Similar to the relativistic case r_w coincides with $r_w^\star$ in the linear-growth regime. The saturation at late times is discontinuous. Here we set $r_0 = 1$.

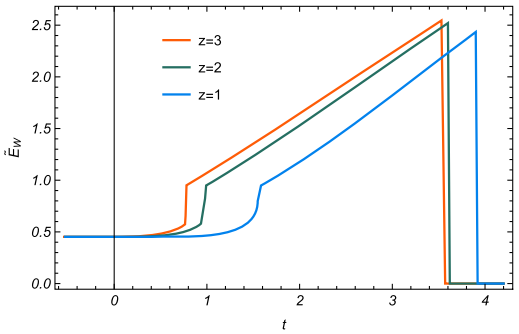

FIG. 7. Evolution of the EWCS for different values of z. Here we set $h = 2.1, \ell = 4$, and $r_0 = 1$.

EWCS for different values of the dynamical exponent when Σ becomes trivial at late times.

V. CONCLUSIONS AND DISCUSSIONS

In this work, we have studied the evolution of information measures dual to the EWCS after a global quantum quench in holographic theories. In our investigations, we have been focused on both relativistic boundary theories as well as non-relativistic ones which has nontrivial Lifshitz and hyperscaling-violating exponents. We present a combination of analytic and numerical results for symmetric strip-shaped boundary subregions which enable us to study different regimes of evolution during the thermalization process.

In the limit of large entangling regions, we realize that the time evolution of EWCS in relativistic theories is characterized by three different scaling regimes; an early time quadratic growth, an intermediate linear growth and a late-time saturation. We found that as the width of the boundary region becomes larger, the region with linear growth becomes more pronounced. Further, in theories with nontrivial dynamical and hyperscaling-violating exponents, the general behavior of the EWCS is very similar to the relativistic case, but in this case, the scaling of the initial growth is not quadratic and depends on z. More explicitly, in this regime we found $E_W \propto t^{1+\frac{1}{z}}$ which show that the scaling of EWCS becomes less pronounced when the dynamical exponent became large. In particular, in $z \to \infty$ limit we have a linear growth regime even in early times. On the other hand, during the intermediate stage of time evolution, EWCS exhibits a linear scaling whose coefficient depends on the thermal entropy density of the final equilibrium state. Motivated by this linear growth and in analogy to the previous results for HEE and the EWCS [52,58] we define a rate of growth

$$\mathcal{R}_W(t) \equiv \frac{1}{\mathcal{S}_{\text{th}} l^{d-2}} \frac{\mathrm{d}E_W}{\mathrm{d}t}. \tag{5.1}$$

Using Eqs. (4.5) and (4.9) we find that for the HSL background

$$\mathcal{R}_W(t) = \begin{cases} \frac{2\pi}{d-1}\frac{\mathcal{E}}{\mathcal{S}_{\text{th}}}(zt)^{\frac{1}{z}} & t \ll r_0 \ll \ell \\ V_W & r_0 \ll t \ll \ell \end{cases}, \tag{5.2}$$

where the entanglement velocity is given by Eq. (4.10). Specifically, We have shown that in nonrelativistic theories i.e., $z > 1$ this velocity depends on the temperature of the final equilibrium state. Indeed, we observe that $V_W \propto T^{\frac{z-1}{z}}$ and hence the larger the value of the temperature is, the faster the EWCS grows in time. Moreover, in the asymptotic limit $z \to \infty$ the rate of growth has a linear dependence on temperature. An interesting question is if either of these behaviors can be extracted from field theory calculations of various boundary information quantifiers dual to the EWCS. Indeed, the time evolution of EE and some other related measures for nonrelativistic field theories with nontrivial Lifshitz exponent has been studied in [59–61]. It would be interesting to figure out what the universal features of entanglement and information evolution in these theories are.

ACKNOWLEDGMENTS

We would like to thank Ali Mollabashi for his collaboration in the early stages of this project.

[1] M. Rangamani and T. Takayanagi, Holographic entanglement entropy, Lect. Notes Phys. **931**, 1 (2017).
[2] T. Nishioka, Entanglement entropy: Holography and renormalization group, Rev. Mod. Phys. **90**, 035007 (2018).
[3] H. Casini and M. Huerta, Lectures on entanglement in quantum field theory, Proc. Sci. TASI2021 (**2023**) 002.
[4] S. Ryu and T. Takayanagi, Holographic Derivation of Entanglement Entropy from AdS/CFT, Phys. Rev. Lett. **96**, 181602 (2006).
[5] V. E. Hubeny, M. Rangamani, and T. Takayanagi, A covariant holographic entanglement entropy proposal, J. High Energy Phys. 07 (2007) 062.
[6] T. Takayanagi and K. Umemoto, Entanglement of purification through holographic duality, Nat. Phys. **14**, 573 (2018).
[7] P. Nguyen, T. Devakul, M. G. Halbasch, M. P. Zaletel, and B. Swingle, Entanglement of purification: From spin chains to holography, J. High Energy Phys. 01 (2018) 098.
[8] S. Dutta and T. Faulkner, A canonical purification for the entanglement wedge cross-section, J. High Energy Phys. 03 (2021) 178.
[9] K. Tamaoka, Entanglement Wedge Cross Section from the Dual Density Matrix, Phys. Rev. Lett. **122**, 141601 (2019).
[10] P. Hayden, M. Lemm, and J. Sorce, Reflected entropy is not a correlation measure, arXiv:2302.10208.
[11] A. C. Wall, Maximin surfaces, and the strong subadditivity of the covariant holographic entanglement entropy, Classical Quantum Gravity **31**, 225007 (2014).
[12] H. Hirai, K. Tamaoka, and T. Yokoya, Towards entanglement of purification for conformal field theories, Prog. Theor. Exp. Phys. **2018**, 063B03 (2018).

[13] K. Babaei Velni, M. R. Mohammadi Mozaffar, and M. H. Vahidinia, Some aspects of entanglement wedge cross-section, J. High Energy Phys. 05 (2019) 200.
[14] N. Jokela and A. Pönni, Notes on entanglement wedge cross sections, J. High Energy Phys. 07 (2019) 087.
[15] K. Umemoto, Quantum and classical correlations inside the entanglement wedge, Phys. Rev. D **100**, 126021 (2019).
[16] C. Akers and P. Rath, Entanglement wedge cross sections require tripartite entanglement, J. High Energy Phys. 04 (2020) 208.
[17] B. Amrahi, M. Ali-Akbari, and M. Asadi, Holographic entanglement of purification near a critical point, Eur. Phys. J. C **80**, 1152 (2020).
[18] S. Chakrabortty, S. Pant, and K. Sil, Effect of back reaction on entanglement and subregion volume complexity in strongly coupled plasma, J. High Energy Phys. 06 (2020) 061.
[19] A. Saha and S. Gangopadhyay, Holographic study of entanglement and complexity for mixed states, Phys. Rev. D **103**, 086002 (2021).
[20] M. Sahraei, M. J. Vasli, M. R. M. Mozaffar, and K. B. Velni, Entanglement wedge cross section in holographic excited states, J. High Energy Phys. 08 (2021) 038.
[21] R. Q. Yang, C. Y. Zhang, and W. M. Li, Holographic entanglement of purification for thermofield double states and thermal quench, J. High Energy Phys. 01 (2019) 114.
[22] Y. Kusuki and K. Tamaoka, Dynamics of entanglement wedge cross section from conformal field theories, Phys. Lett. B **814**, 136105 (2021).
[23] H. S. Jeong, K. Y. Kim, and M. Nishida, Reflected entropy and entanglement wedge cross section with the first order correction, J. High Energy Phys. 12 (2019) 170.
[24] Y. Kusuki and K. Tamaoka, Entanglement wedge cross section from CFT: Dynamics of local operator quench, J. High Energy Phys. 02 (2020) 017.
[25] J. Kudler-Flam, Y. Kusuki, and S. Ryu, Correlation measures and the entanglement wedge cross-section after quantum quenches in two-dimensional conformal field theories, J. High Energy Phys. 04 (2020) 074.
[26] M. Moosa, Time dependence of reflected entropy in conformal field theory, J. High Energy Phys. 05 (2020) 082.
[27] J. Boruch, Entanglement wedge cross-section in shock wave geometries, J. High Energy Phys. 07 (2020) 208.
[28] S. Khoeini-Moghaddam, F. Omidi, and C. Paul, Aspects of hyperscaling violating geometries at finite cutoff, J. High Energy Phys. 02 (2021) 121.
[29] P. Bueno and H. Casini, Reflected entropy, symmetries and free fermions, J. High Energy Phys. 05 (2020) 103.
[30] A. Mollabashi and K. Tamaoka, A field theory study of entanglement wedge cross section: Odd entropy, J. High Energy Phys. 08 (2020) 078.
[31] C. Berthiere, H. Chen, Y. Liu, and B. Chen, Topological reflected entropy in Chern-Simons theories, Phys. Rev. B **103**, 035149 (2021).
[32] P. Bueno and H. Casini, Reflected entropy for free scalars, J. High Energy Phys. 11 (2020) 148.
[33] H. A. Camargo, L. Hackl, M. P. Heller, A. Jahn, and B. Windt, Long-Distance Entanglement of Purification and Reflected Entropy in Conformal Field Theory, Phys. Rev. Lett. **127**, 141604 (2021).
[34] Q. Wen, Balanced partial entanglement and the entanglement wedge cross section, J. High Energy Phys. 04 (2021) 301.
[35] A. R. Chowdhury, A. Saha, and S. Gangopadhyay, Entanglement wedge cross-section for noncommutative Yang-Mills theory, J. High Energy Phys. 02 (2022) 192.
[36] P. Hayden, O. Parrikar, and J. Sorce, The Markov gap for geometric reflected entropy, J. High Energy Phys. 10 (2021) 047.
[37] C. Akers, T. Faulkner, S. Lin, and P. Rath, Reflected entropy in random tensor networks, J. High Energy Phys. 05 (2022) 162.
[38] H. A. Camargo, P. Nandy, Q. Wen, and H. Zhong, Balanced partial entanglement and mixed state correlations, SciPost Phys. **12**, 137 (2022).
[39] D. Basu, H. Parihar, V. Raj, and G. Sengupta, Entanglement negativity, reflected entropy, and anomalous gravitation, Phys. Rev. D **105**, 086013 (2022); **105**, 129902(E) (2022).
[40] J. K. Basak, H. Chourasiya, V. Raj, and G. Sengupta, Reflected entropy in Galilean conformal field theories and flat holography, Eur. Phys. J. C **82**, 1169 (2022).
[41] A. Chowdhury Roy, A. Saha, and S. Gangopadhyay, Mixed state information theoretic measures in boosted black brane, Ann. Phys. (Amsterdam) **452**, 169270 (2023).
[42] M. J. Vasli, M. R. Mohammadi Mozaffar, K. Babaei Velni, and M. Sahraei, Holographic study of reflected entropy in anisotropic theories, Phys. Rev. D **107**, 026012 (2023).
[43] J. Abajo-Arrastia, J. Aparicio, and E. Lopez, Holographic evolution of entanglement entropy, J. High Energy Phys. 11 (2010) 149.
[44] T. Albash and C. V. Johnson, Evolution of holographic entanglement entropy after thermal and electromagnetic quenches, New J. Phys. **13**, 045017 (2011).
[45] V. Balasubramanian, A. Bernamonti, J. de Boer, N. Copland, B. Craps, E. Keski-Vakkuri, B. Müller, A. Schäfer, M. Shigemori, and W. Staessens, Thermalization of Strongly Coupled Field Theories, Phys. Rev. Lett. **106**, 191601 (2011).
[46] H. Liu and S. J. Suh, Entanglement Tsunami: Universal Scaling in Holographic Thermalization, Phys. Rev. Lett. **112**, 011601 (2014).
[47] H. Casini, H. Liu, and M. Mezei, Spread of entanglement and causality, J. High Energy Phys. 07 (2016) 077.
[48] M. Alishahiha, A. Faraji Astaneh, and M. R. Mohammadi Mozaffar, Thermalization in backgrounds with hyperscaling violating factor, Phys. Rev. D **90**, 046004 (2014).
[49] P. Fonda, L. Franti, V. Kernen, E. Keski-Vakkuri, L. Thorlacius, and E. Tonni, Holographic thermalization with Lifshitz scaling and hyperscaling violation, J. High Energy Phys. 08 (2014) 051.
[50] S. Leichenauer and M. Moosa, Entanglement tsunami in $(1+1)$-dimensions, Phys. Rev. D **92**, 126004 (2015).
[51] M. Alishahiha, M. R. Mohammadi Mozaffar, and M. R. Tanhayi, On the time evolution of holographic n-partite information, J. High Energy Phys. 09 (2015) 165.

[52] K. Babaei Velni, M. R. Mohammadi Mozaffar, and M. H. Vahidinia, Evolution of entanglement wedge cross section following a global quench, J. High Energy Phys. 08 (2020) 129.

[53] C. Keeler, G. Knodel, and J. T. Liu, What do non-relativistic CFTs tell us about Lifshitz spacetimes?, J. High Energy Phys. 01 (2014) 062.

[54] S. A. Gentle and C. Keeler, On the reconstruction of Lifshitz spacetimes, J. High Energy Phys. 03 (2016) 195.

[55] M. Alishahiha, E. O. Colgain, and H. Yavartanoo, Charged black branes with hyperscaling violating factor, J. High Energy Phys. 11 (2012) 137.

[56] M. Alishahiha and A. Faraji Astaneh, Complexity of hyperscaling violating theories at finite cutoff, Phys. Rev. D **100**, 086004 (2019).

[57] X. Dong, S. Harrison, S. Kachru, G. Torroba, and H. Wang, Aspects of holography for theories with hyperscaling violation, J. High Energy Phys. 06 (2012) 041.

[58] H. Liu and S. J. Suh, Entanglement growth during thermalization in holographic systems, Phys. Rev. D **89**, 066012 (2014).

[59] M. R. Mohammadi Mozaffar and A. Mollabashi, Entanglement evolution in Lifshitz-type scalar theories, J. High Energy Phys. 01 (2019) 137.

[60] M. R. Mohammadi Mozaffar and A. Mollabashi, Universal scaling in fast quenches near Lifshitz-like fixed points, Phys. Lett. B **797**, 134906 (2019).

[61] M. R. M. Mozaffar and A. Mollabashi, Time scaling of entanglement in integrable scale-invariant theories, Phys. Rev. Res. **4**, L022010 (2022).